



**Template and surfactant free synthesis of hierarchical
WO₃•0.33H₂O via a facile solvothermal route for
photocatalytic RhB degradation**

Journal:	<i>CrystEngComm</i>
Manuscript ID:	CE-ART-02-2014-000361.R1
Article Type:	Paper
Date Submitted by the Author:	19-Mar-2014
Complete List of Authors:	Zheng, Yi; Harbin Institute of Technology, Department of Chemistry Chen, Gang; Harbin Institute of Technology, Department of Chemistry Yu, Yao-Guang; Harbin Institute of Technology (HIT), Department of chemistry Sun, Jingxue; Harbin Institute of Technology, Department of Chemistry zhou, yansong; Harbin Institute of Technology, Department of Chemistry Pei, Jian; Harbin Institute of Technology, Department of Chemistry

ARTICLE

Template and surfactant free synthesis of hierarchical $\text{WO}_3 \cdot 0.33\text{H}_2\text{O}$ via a facile solvothermal route for photocatalytic RhB degradation

Cite this: DOI: 10.1039/x0xx00000x

Yi Zheng, Gang Chen, * Yaoguang Yu, Jingxue Sun, Yansong Zhou, Jian Pei

Received 00th January 2012,
Accepted 00th January 2012

DOI: 10.1039/x0xx00000x

www.rsc.org/

A template- and surfactant-free solvothermal method has been successfully developed for the controlled synthesis of 3D micro-dahlia $\text{WO}_3 \cdot 0.33\text{H}_2\text{O}$ hierarchical structure with single-crystalline petal for the first time. In this reaction system, acetone have played a key role due to high saturated vapour pressure, high solubility of precursor, low solvent polarity, and its organic groups. The optimum volume ratio of water and acetone is 2 to 1 for the formation of perfect micro-dahlia hierarchical structure. Based on the scan electron microscope and transmission electron microscope observations and experiment results, the reaction process and growth mechanism of such hierarchitcture were proposed. Moreover, UV-Vis absorption measurements demonstrated that visible light absorption of the products increased gradually with the increasing volume of acetone. Photocatalytic activity of micro-dahlia $\text{WO}_3 \cdot 0.33\text{H}_2\text{O}$ displayed higher than the sample synthesized using water as solvent. After 240 minutes photodegradation process, 88.5% of RhB was eliminated by hierarchical micro-dahlia $\text{WO}_3 \cdot 0.33\text{H}_2\text{O}$.

1 Introduction

Recently, synthesis of hierarchical structure functional materials has been an attractive way in many fields, such as sensor,¹⁻⁴ catalyst,⁵⁻⁸ lithium ion battery,⁹⁻¹² electrochromic device,¹³⁻¹⁵ photochromic device,¹⁶ etc. Due to their special structure, they usually exhibit unique properties. A number of inorganic materials with hierarchical structures have been fabricated in such a purpose. Nonetheless, directionally assemble the blocks into a hierarchical structure is generally difficult and requires further study to improve. In most of synthesis methods, templates are usually required for their growth.^{17,18} However, the templates will increase the difficulty of after-treatment, introduce impurities, and even increase costs.¹⁹⁻²¹ Therefore, the development of facile, template-free, and self-assembly routes for the formation of hierarchical structure of various types of semiconductor is still a hot research.²⁰⁻²⁴

Tungsten trioxide hydrates ($\text{WO}_3 \cdot n\text{H}_2\text{O}$, $n = 0\sim 2$) with hierarchical structure, as one of the important transition metal oxides,²⁵⁻²⁸ have been rarely reported for studying their photocatalytic properties. Therefore, it is necessary to study the synthesis method of hierarchical structure tungsten trioxide hydrates and investigate their photocatalytic properties. Considering tungsten trioxide hydrates and tungsten trioxide are counterparts, the synthesis method can be also applicable in

synthesis of tungsten trioxide. For $\text{WO}_3 \cdot 0.33\text{H}_2\text{O}$, several hierarchical structures have been reported. hexagonal-shaped $\text{WO}_3 \cdot 0.33\text{H}_2\text{O}$ nanodiscs which were composed of nanosheets had been prepared by Zhou et al.²⁹ Yang et al.²⁵ synthesized hierarchical chrysanthemum-like $\text{WO}_3 \cdot 0.33\text{H}_2\text{O}$. And $\text{WO}_3 \cdot 0.33\text{H}_2\text{O}$ hierarchical nanonetworks was synthesized by He et al.²⁶ There are also other hierarchical structures, such as hierarchical $\text{WO}_3 \cdot 0.33\text{H}_2\text{O}$ mesoporous nanorod assemblies,²⁸ hierarchically structured snowflakelike $\text{WO}_3 \cdot 0.33\text{H}_2\text{O}$.³⁰ These $\text{WO}_3 \cdot 0.33\text{H}_2\text{O}$ are all synthesized in water system with additives. In addition, $\text{WO}_3 \cdot 0.33\text{H}_2\text{O}$ hierarchical structure had been synthesized by mixed solvent. Ma et al.³¹ obtained $\text{WO}_3 \cdot 0.33\text{H}_2\text{O}$ hierarchical microstructures via a facile microwave-assisted solvothermal route employing water and glycol mixed solvent and disodium ethylenediaminetetraacetic ($\text{Na}_2\text{H}_2\text{EDTA}$) as a structure-directing agent. However, these hierarchically structures are all obtained in the presence of additives. To the best of our knowledge, there has been no report of the preparation of assembled $\text{WO}_3 \cdot 0.33\text{H}_2\text{O}$ hierarchical microstructures via a facile solvothermal method without any additive.

Acetone is a common solvent, and it represents an important structural type in a variety of chemical reactions and interactions based on its carbonyl group.³²⁻³⁴ Surface hydroxyl groups of metal oxide can form hydrogen-bonds with adsorbed

acetone molecules, and acetone can also be adsorbed on semiconductor surface by carbonyl group and active α -hydrogen directly interacted with metal cations and oxygen anions. This interaction will affect the crystal growth process. In addition, other factors, such as solubility of precursors in solvent, polarity of solvent, saturated vapor pressure, could also affect the crystal growth process.^{35,36} These could be achieved by adjusting solvent. Herein, we have successfully synthesized $\text{WO}_3 \cdot 0.33\text{H}_2\text{O}$ hierarchical microstructures based on solvothermal method by using water and acetone as solvent. The experimental results showed that water and acetone have both played key roles on morphology of $\text{WO}_3 \cdot 0.33\text{H}_2\text{O}$. Some reaction parameters such as reaction time, volume of acetone were systematically investigated. Based on the experimental results, micro-dahlia hierarchical structures formation process was given. Finally, photocatalytic activity of micro-dahlia like $\text{WO}_3 \cdot 0.33\text{H}_2\text{O}$ was investigated. This work might provide a potential synthesis method for tungsten trioxide counterparts and the materials closed to tungsten trioxide, such as molybdenum trioxide.

2 Experimental

2.1 Materials

Sodium tungstate dihydrate ($\text{Na}_2\text{WO}_4 \cdot 2\text{H}_2\text{O}$, AR) of $\geq 99.5\%$ purity was purchased from Sinopharm Chemical Reagent Co., Ltd. Hydrochloric acid and acetone are analytical reagent purchased from Sinopharm Chemical Reagent Co., Ltd. And ultra-pure water is homemade (18.2 M Ω .cm, CSR-1-10, Beijing Aisitaik Technology Development Co., Ltd.).

2.2 Synthesis of hierarchical $\text{WO}_3 \cdot 0.33\text{H}_2\text{O}$

In typically, $\text{Na}_2\text{WO}_4 \cdot 2\text{H}_2\text{O}$ (0.5 g, 1.516 mmol) were dissolved in 33 mL of ultra-pure water at room temperature. 0.43 mL of 38% HCl was added slowly and carefully, a bit yellow clear H_2WO_4 collosol was obtained. Then above solution was placed into a Teflon-lined stainless steel autoclave, which was sealed and maintained at 140 °C for 72 h, then rinsed with deionized water several times and dried at 60 °C, labelled as **WS**. Micro-dahlia $\text{WO}_3 \cdot 0.33\text{H}_2\text{O}$ will be obtained by replacing 11 mL of ultra-pure water with 11 mL of acetone, labelled as **WF1**.

2.3 Characterization

The collected products were characterized by powder X-ray diffractometer (Rigaku D/max-2000) with Cu K α radiation at a scanning rate of 5° min⁻¹ in the 2 θ range of 10°–90°. The morphology of the products were observed by FESEM (Helios Nanolab600i), TEM, HRTEM, and SAED were carried out on FEI TecnaiG2F30, UV–vis diffuse reflectance spectra were acquired by a spectrophotometer (TU-1900) and BaSO₄ was used as the reflectance standard.

2.4 Photocatalytic activity measurement

In this measurement, a 300W Xe lamp (Trustech PLS-SXE 300, Beijing) was used as light source, and 10 mg·L⁻¹ RhB aqueous solution, as a representative compound in waste water, was used as target photodegradation pollutant in heterogeneous photocatalysis reaction. In each experiment, a quartz beaker containing 100 ml of RhB aqueous solution and 50 mg of photocatalyst was firstly put into an ultrasonic bath to disperse photocatalyst under dark 10 min, and then stirred 40 min in dark continuously in order to achieve adsorption–desorption equilibrium. The concentration of RhB during the degradation process was monitored by colorimetry using a UV-vis spectrometer (TU-1900) every 20 min, which obtained by being centrifuged at 10,000 rpm for 5 min.

3 Results and discussion

3.1 Phase composition and microstructure

As-prepared tungsten trioxide hydrates have been synthesized via hydrothermal and solvothermal. The products was labelled as WS and WFs, as seen in Tab. 1.

The phase purity and the crystallographic structure of the products were determined by X-ray diffraction (XRD), as shown in Fig.1. All of the detected peaks of two samples could be well indexed to the orthorhombic structure with the Fmm2(42) space group (JCPDS Card No. 87-1203), indicating the samples had been successfully synthesized by the hydrothermal and solvothermal route, respectively. There were not existing impurities, and the sharp diffraction peaks described good crystallization. Typical low-magnification SEM image showed that the majority morphologies of the products were numerous micro-dahlias (Fig. 2a) and micro-thorn spheres (Fig. 2c), respectively. More detailed morphologies (Fig. 2b, 2d) demonstrated that the dahlia like hierarchical structure consist of micro-hexagonal platelets which were ordered and some misplaced face-to-face aligned into micro-dahlia, and micro-thorn sphere was consisted of center orientation gathered micro-rods or micro-rectangular plates. Details of the hierarchical structures could also be seen in the TEM images as shown in Fig. 3. The detailed information from the edge of the sample was observed. Combined with Fig. 2b, 2d and Fig. 3b, 3d, it was shown that the block unit of WF1 synthesized in water and acetone system more tended to get pseudo-regular hexagonal plates. While, the block unit of WS synthesized in water system more tended to get rectangular-like hexagonal plates. Acetone played a key role in controlling the morphology of $\text{WO}_3 \cdot 0.33\text{H}_2\text{O}$. High-resolution TEM (HRTEM) and selected area electron diffraction (SAED) (test area was labeled with a circle in Fig. 3b, 3d) suggested that the blocks of both samples

Tab. 1 The short name of synthesized cubic tungsten trioxide hemihydrates with different synthesis conditions.

short name	water	acetone
WS	33 mL	0 mL
WF1	11 mL	22 mL

WF2	16.5 mL	16.5 mL
WF3	22 mL	11 mL

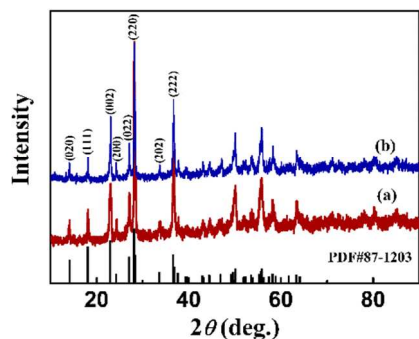


Fig. 1 X-ray diffraction patterns of (a) WS, (b) WF1.

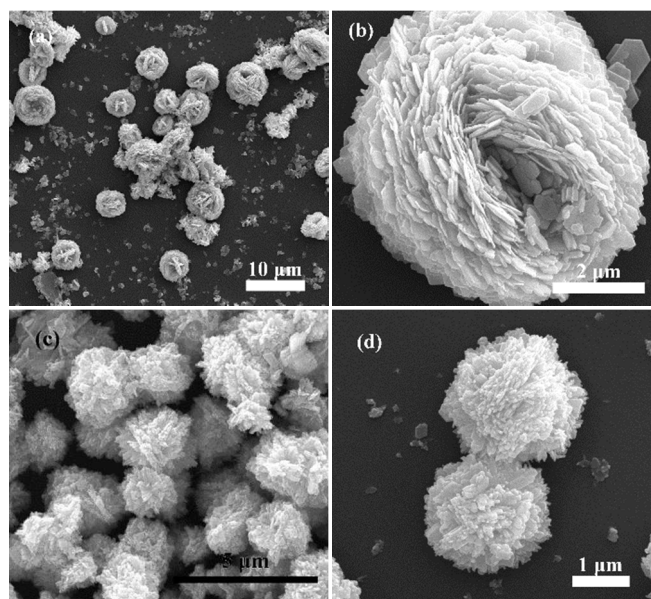


Fig. 2 SEM images of $\text{WO}_3 \cdot 0.33\text{H}_2\text{O}$ samples prepared in different system, (a,b) WF1, (c,d) WS.

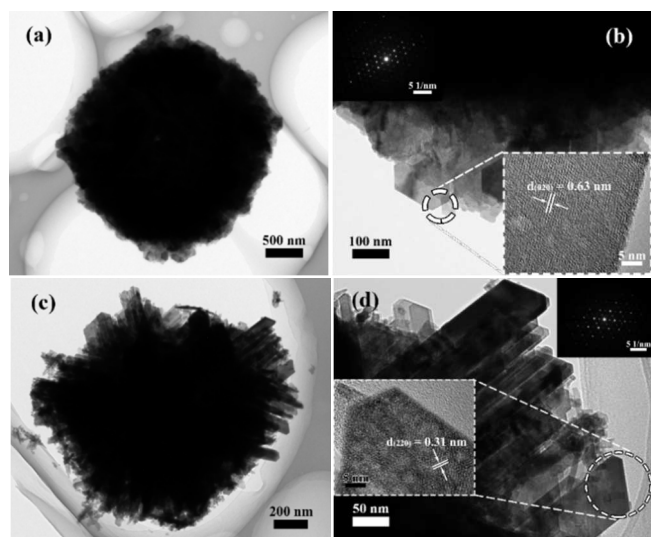


Fig. 3 TEM images of $\text{WO}_3 \cdot 0.33\text{H}_2\text{O}$ samples prepared in different system, (a, b) WF1, (c, d) WS.

were all monocrystallines. And the well-resolved 2D diffraction fringes among the different samples unit were uniform with a plane spacing of 0.63 nm (corresponds to the (020) lattice planes) for WF1, a plane spacing of 0.31 nm (corresponds to the (220)

lattice planes) for WS. Some holes could be seen from the HRTEM images, due to loss of crystal water under electron beam irradiation, which could be clearly seen in Fig. S1. This phenomenon could be used to prepare mesoporous tungsten oxides for some applications.

Generally, crystal growth is affected by intrinsic crystal structure and external reaction conditions.³⁵ The variety of external factors, such as the properties of the solvent, could impact on the growth process of semiconductor under solvothermal condition. Solubility of precursor in solvent is an important factor. High solubility would induce the nucleation more uniform. Acidified sodium tungstate had high solubility in mixed solvent of water and acetone. In addition, carbonyl oxygen of acetone is electronegative which can interact with tungsten ion. While, α -hydrogen of acetone is active and may interact with the oxygen ion which is adjacent to the tungsten ion. It is similar to the interaction between acetone and Ge, Si or TiO_2 .^{29, 34, 37} In water system, (220) crystal planes were exposed due to the intrinsic crystal structure of $\text{WO}_3 \cdot 0.33\text{H}_2\text{O}$. (020) crystal planes were exposed in water and acetone system. It was shown that acetone tended to interact with the exposed ions in (020). Such interaction allowed to retain the (020) crystal planes. So that the long hexagonal plates changed into short hexagonal plates when

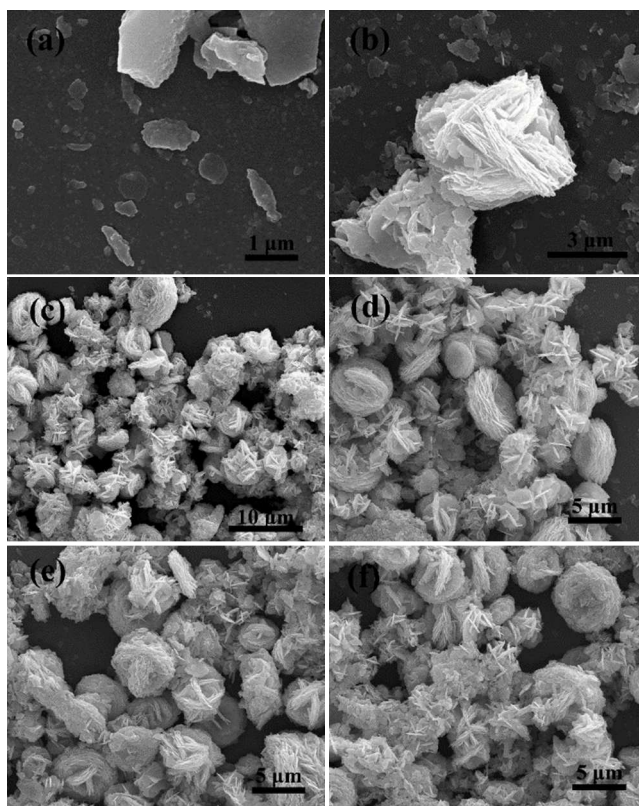


Fig. 4 SEM images of the products obtained at various reaction stages: (a) 1 h, (b) 2 h, (c) 3 h, (d) 5 h, (e) 8 h, (f) 12 h.



Fig. 5 Growth mechanism schematic diagram of micro-dahlia $\text{WO}_3 \cdot 0.33\text{H}_2\text{O}$

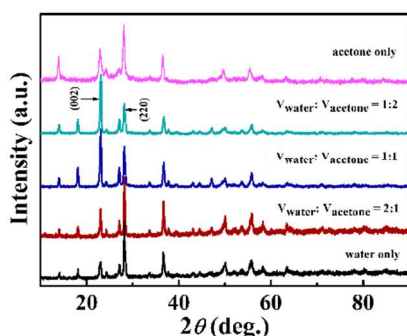


Fig. 6 X-ray diffraction patterns of as-prepared samples which in different volume ratio of water and acetone.

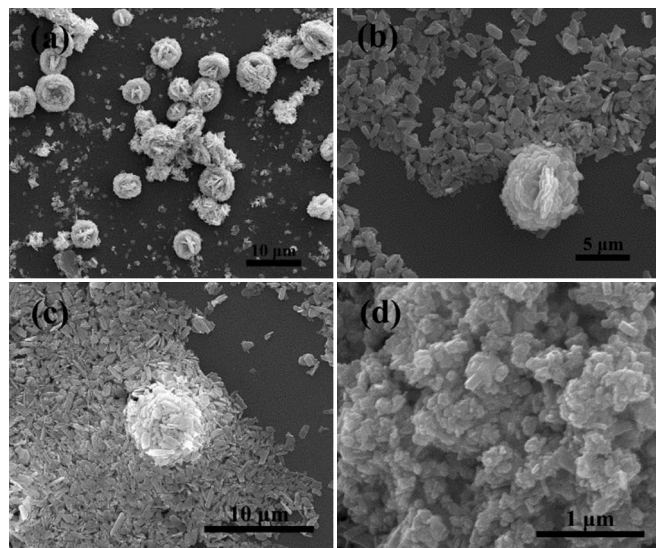


Fig. 7 SEM images of $\text{WO}_3 \cdot 0.33\text{H}_2\text{O}$ samples prepared in different systems, (a) only water used as solvent, (b) mixed solvent ($V_{\text{water}} : V_{\text{acetone}} = 2 : 1$), (c) mixed solvent ($V_{\text{water}} : V_{\text{acetone}} = 1 : 1$), (d) mixed solvent ($V_{\text{water}} : V_{\text{acetone}} = 1 : 2$), (e) only acetone used as solvent.

acetone was added. This is why there were two kinds of unit block morphologies of $\text{WO}_3 \cdot 0.33\text{H}_2\text{O}$. Due to the different

morphologies of blocks and reaction environment which were induced by acetone, the final product has different morphologies.

3.2 Growth process

In order to understand the growth process of WF1 specimen, time-dependent experiments were carried out just at different reaction time without changing the 2:1 volume ratio of water and acetone. The SEM results were shown in Fig. 2, it could be seen that micro-sheets were obtained within the first hour. The sample was white precipitate, and be dried to give a yellowish transparent film. Reaction was continued for another hour, it was found the sheet structures grew bigger and occurred aggregation with each other. The state of aggregation of sheet structures tended to have a face-to-face stack into an erythrocyte structure, and these erythrocytes might randomly occur interleaved with each other. Continued to extend the reaction time to 3 h, complete dahlia-shaped hierarchical structures were obtained. There were two kinds of dahlia-shaped hierarchical structure. Due to the random aggregation of the erythrocyte structures, this is why micro-dahlia hierarchical structures with or without stamen could be found at the same time. And this dahlia-shaped hierarchical structures gradually increased and perfected after 5-12 hours reaction time. Observed carefully, the micro-sheets (ca. 25 nm thick) were roughness at the beginning of the reaction (0-3h) in Fig. S2(a). The side of each micro-sheet was wavy. But these thin sheet structures became smooth after longer reaction time. After 5 h reaction time, the wavy sides of micro-sheet became smooth, and the edge thick of micro-plate was ca. 50 nm, as shown in Fig. S2(b). After the 72 h reaction, perfect single wafer (with perfect edges) was obtained. Based on the above analysis, a possible simple growth mechanism schematic diagram was proposed and shown in Fig. 5.

3.3 Effect of acetone

According to the above analysis, acetone played a key role on morphology of $\text{WO}_3 \cdot 0.33\text{H}_2\text{O}$ in such a reaction system of synthesis of $\text{WO}_3 \cdot 0.33\text{H}_2\text{O}$ micro-dahlia hierarchical structure. This could be understood through XRD patterns (Fig. 1), SEM images (Fig. 2), and TEM images (Fig. 3). To investigate the effect of acetone on morphology evolution, a control experiment with different volume of acetone was carried out during 72 h. Fig. 6 showed the XRD patterns of as-prepared samples which in different volume ratio of water and acetone. Observed carefully, the intensity of (002) diffraction peak was gradually increased with increasing the acetone. It is shown that the orientation of (002) was increased. In the absence of acetone, micro-thorn sphere was formed, which was consisted of centre orientation gathered micro-rods and micro-long plates. When 11 ml of water was replaced with 11 ml of acetone, entirely different micro-dahlia was obtained, and the shape of block unit was also changed from rod-like or long plate-like

blocks of WS to more pseudo-regular hexagonal plate blocks of WF1 (Fig. 2a). When 16.5 ml of water was replaced with 16.5 ml of acetone, micro-dahlia could also be obtained and some petals were obtained at the same time (Fig. 7b), and this sample was labelled as **WF2**. Continuing to increase the relative content of acetone to 22 ml, a large amount of petals were obtained and only a small amount micro-dahlia remaining (Fig. 7c), labelled as **WF3**. Meanwhile, it could also be shown that shape of petal was changed with increasing amounts of acetone. Hexagonal petals began to become narrow. If water was all replaced with acetone, only rectangular rods were obtained (Fig. 7d). The XRD pattern (Fig. 6) of sample synthesized in pure acetone was indexed to hexagonal phase of $\text{WO}_3 \cdot 0.33\text{H}_2\text{O}$ (JCPDS Card No. 35-1001).³⁸ The phase and morphology of the sample were all changed when water was not added.

Adding acetone would change the properties of the reaction solution, such as solubility of the precursors³⁵, saturated vapour pressure³⁶, viscosity³⁹ *etc.* In this work, solubility of the precursors are high in mixed solvent (water and acetone), but very low in acetone. From Fig. 7d, it can be seen that the sample, which was synthesized by using acetone, has inhomogeneous morphology. This may be induced by the non-uniform nucleation. Furthermore, tungstate anions were considered a precursor of tungsten oxide.⁴⁰⁻⁴³ The solubility of sodium tungstate would directly affect the existence state of tungstate anions. This is the reason hexagonal phase of $\text{WO}_3 \cdot 0.33\text{H}_2\text{O}$ was obtained when using acetone as solvent, and orthorhombic phase of $\text{WO}_3 \cdot 0.33\text{H}_2\text{O}$ were obtained in water and acetone reaction system, respectively. Xu *et al.*³⁵ believed that crystal growth habit depends on interface-solvent interactions. The interactions would be weaker in lower polarity solvents, leading to less anisotropic growth rates and more equi-axed ZnO crystals.⁴⁴ This result is similar to this work. When acetone was added, the polarity of solvent was decreased. Thus, short and equi-axed hexagonal plate unit was obtained (compared with WS). As mentioned above, petals gradually began to become narrow with increasing the amount of acetone. It would be due to the mass transfer rate of reactive substances is larger in the reaction system which contains more water, it tend to form more equi-axed petal. Compared with WS, WFs have shorter hexagonal plate units. In addition, saturated vapour pressure is also an important factor to affect the growth of crystal. When saturated vapour pressure of solvent became higher by increasing the volume of acetone, petals increased. It is due to the higher boiling point of the solvent, which would induce low level of amalgamation of the nucleus.³⁶ Thus, it is easier to form an individual pattern than hierarchical structure (micro-dahlia). Generally, it is shown that water and acetone were indispensable, and perfect micro-dahlia like hierarchical structure was obtained when 2:1 volume ratio of water and acetone was used as solvent.

3.4 Optical Property

Fig. 8 shows the UV-vis absorption spectra of the as-prepared $\text{WO}_3 \cdot 0.33\text{H}_2\text{O}$ hierarchical structures. Adding acetone

significantly affects the optical property of light absorption for as-prepared samples. Though the maximum absorption edge of samples had slight blue shift, the addition of acetone induced the greatly increased light absorption intensity in the visible region (400 nm - 700 nm),⁴⁵ as observed in all of the micro-dahlia samples with different addition ratios of acetone. It is shown that utilization efficiency of light increased with increasing the volume of acetone. It could be known that petal was increased with increasing the amount of acetone (Fig. 7), and the color of samples gradually deepened (Fig. 8). The phenomenon may be caused by their morphology which could be understood by the exposed planes of themselves. Compared with petal, dahlia exposed more edge surface of petal, which might have a weaker absorption performance. Thus, visible light absorbance of samples gradually increased with petals gradually increased (which was equivalent to the increase amount of acetone).

3.5 Photocatalytic property

Finally, the photocatalytic activity of as-prepared samples were measured by photodegradation of RhB. Fig. 9a showed the photodegradation curve of RhB solutions in the existence of the as-prepared tungsten oxides under 300W Xe lamp illumination, and the time-dependent absorption spectra of the RhB solution were shown in Fig. S3. The absorbance decreases by ca. 3% is the dark-adsorption of WS and ca. 5% for WF1. In order to investigate the photocatalytic activity difference of as-prepared specimens, tests were scheduled for 140 minutes. The maximum absorption wavelength of RhB occurred very slight blue shift, but de-ethylation process didn't happen, due to the wavelength

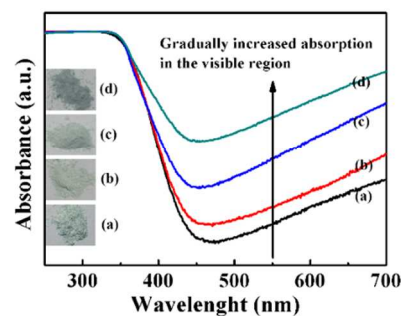


Fig. 8 UV - visible absorption spectra of tungsten oxides prepared in different system, (a) only water used as solvent, mixed solvent (water : acetone) in different volume ratio (b) 2 : 1, (c) 1 : 1, (d) 1 : 2.

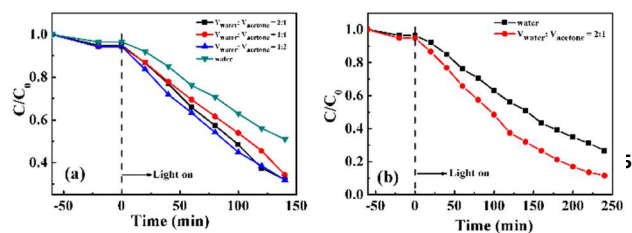


Fig. 9 Degradation of RhB under 300W Xe lamp illumination by as-prepared samples, (a) 140min, (b) 240min, (c) recycled photodegradation of RhB, (d) pump N₂, add methanol, no additive.

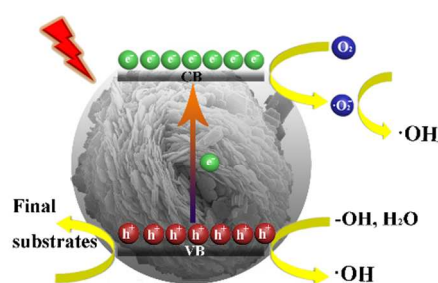


Fig. 10 photocatalytic degradation process diagram of $\text{WO}_3 \cdot 0.33\text{H}_2\text{O}$.

was greater than 539 nm (corresponding to N,N,N'-triethylated rhodamine).⁴⁶⁻⁴⁸ Therefore, it could be considered the entire photodegradation process was a direct cycloreversion or mineralization process. After 140 minutes photodegradation, 49% of RhB was eliminated for WS, and 68% of RhB was eliminated for WF1. WF1 had higher photocatalytic activity may be due to the exposure of (020) as shown in Fig 3b.³⁰ In addition, further study was carried out by extending photocatalytic reaction time to investigate whether RhB could be photocatalytic degradation further. Results were shown in Fig. 9b. After 240 minutes of illumination, 73.4% of RhB was eliminated for WS, and 88.5% of RhB was eliminated for WF1. It is shown that products could be more thorough removal of RhB when prolong the exposure time. Recycle performance is an important indicator of the practical application. Fig. 9c showed the results of recycled photodegradation of RhB without stopping. It can be seen that WF1 displayed an excellent stability after the eight cycles. It is acknowledged that pollutants would be eliminated by photo-generated holes and reactive oxygen species, such as superoxide radicals, and hydroxyl radicals. Superoxide radicals would be directly generated by photo-generated electrons. In order to know which kinds of photo-generated carriers played a role when WF1 was used as the photocatalyst for photodegradation of RhB. The photodegradation mechanism experiment was carried out by

adding methanol, and pumping nitrogen, which were used as wildly and highly efficient quenchers for holes, superoxide radicals, respectively.^{49, 50} Fig 9d showed that pumping nitrogen could be decreased the photocatalytic activity, but the inhibition was strengthened when adding methanol. It is shown that photo-generated electrons played a certain role on photodegradation reaction and photo-generated holes played a major role. From the above results, it could be understood that WF which was exposed (020) lattice planes played better photocatalytic activity compared with WS, displayed excellent stability, and photo-generated holes played a key role during the whole photocatalysis. Possible reactions of the degradation process could be represented in brief, as shown in Fig. 10.

4 Conclusions

In summary, a facile solvothermal method has been developed for the synthesis of 3D micro-dahlia $\text{WO}_3 \cdot 0.33\text{H}_2\text{O}$ hierarchical structure by adding acetone without any additive. Based on high-resolution TEM results, (020) lattice planes were exposed when adding acetone. It is indicated that carbonyl group and α -hydrogen of acetone could interact with the ions (W and O) in (020) crystal plane which lead the (020) crystal planes were reserved. In addition, adding acetone would change the properties of the reaction system, such as solubility of the precursors, saturated vapour pressure, polarity of solvent, etc. These changes eventually led to the formation of 3D micro-dahlia $\text{WO}_3 \cdot 0.33\text{H}_2\text{O}$ hierarchical structure. The optimum volume ratio of water and acetone for forming the perfect micro-dahlia hierarchical structure is 2 to 1 in this work. Moreover, UV-Vis absorption measurements demonstrated that visible light absorption of the products increased gradually with the increasing volume of acetone. Whereas, photocatalytic activity of micro-dahlia $\text{WO}_3 \cdot 0.33\text{H}_2\text{O}$ displayed higher than sample synthesized using water as solvent. The higher photocatalytic activity of WF1 is due the exposed (020) facets. After 240 minutes photodegradation process, 88.5% of RhB was eliminated by hierarchical micro-dahlia $\text{WO}_3 \cdot 0.33\text{H}_2\text{O}$.

Acknowledgements

This work was financially supported by projects of Natural Science Foundation of China (21271055).

Notes and references

Department of Chemistry, Harbin Institute of Technology, Harbin 150001, P. R. China. E-mail: gchen@hit.edu.cn; Fax: +86-451-86413753; Tel: +86-0451-86413753

†Electronic Supplementary Information (ESI) available: TEM images of surface of the sample with the extension of the electron beam irradiation time, due to loss of crystal water. SEM images of edges of WF1 sample with different reaction time. UV-vis adsorption spectral changes of the RhB solution ($10 \text{ mg} \cdot \text{L}^{-1}$) over as-prepared samples by simulated sunlight irradiation. See DOI: 10.1039/b000000x/

1. D. Wang, S. Du, X. Zhou, B. Wang, J. Ma, P. Sun, Y. Sun and G. Lu, *CrystEngComm*, 2013, **15**, 7438-7442.

2. H. Wang, K. Dou, W. Y. Teoh, Y. Zhan, T. F. Hung, F. Zhang, J. Xu, R. Zhang and A. L. Rogach, *Adv. Funct. Mater.* 2013, **23**, 4847-4853.
3. Y. Qin, G. Fan, K. Liu and M. Hu, *Sensor. Actuat. B: Chem.* 2014, **190**, 141-148.
4. J. Zai, J. Zhu, R. Qi and X. Qian, *J. Mater. Chem. A*, 2013, **1**, 735-745.
5. P. Madhusudan, J. Zhang, B. Cheng and G. Liu, *CrystEngComm*, 2013, **15**, 231-240.
6. C. M. A. Parlett, K. Wilson and A. F. Lee, *Chem. Soc. Rev.* 2013, **42**, 3876-3893.
7. Z. Guo, D. Zhou, X. Dong, Z. Qiu, Y. Wang and Y. Xia, *Adv. Mater.* 2013, **25**, 5668-5672.
8. Z. M. Cui, Z. Chen, C. Y. Cao, W. G. Song and L. Jiang, *Chem. Commun.* 2013, **49**, 6093-6095.
9. S. Liu, J. Wang, J. Wang, F. Zhang, F. Liang and L. Wang, *CrystEngComm*, 2014, **16**, 814-819.
10. D. Lei, M. Zhang, B. Qu, J. Ma, Q. Li, L. Chen, B. Lu and T. Wang, *Electrochim. Acta*, 2013, **106**, 386-391.
11. J. M. Jeong, B. G. Choi, S. C. Lee, K. G. Lee, S. J. Chang, Y.-K. Han, Y. B. Lee, H. U. Lee, S. Kwon, G. Lee, C.-S. Lee and Y. S. Huh, *Adv. Mater.* 2013, **25**, 6250-6255.
12. S. H. Lee, V. Sridhar, J. H. Jung, K. Karthikeyan, Y. S. Lee, R. Mukherjee, N. Koratkar and I.-K. Oh, *ACS Nano*, 2013, **7**, 4242-4251.
13. D. Ma, G. Shi, H. Wang, Q. Zhang and Y. Li, *Nanoscale*, 2013, **5**, 4808-4815.
14. G. F. Cai, X. L. Wang, D. Zhou, J. h. Zhang, Q. Q. Xiong, C. D. Gu and J. P. Tu, *RSC Adv.* 2013, **3**, 6896-6905.
15. G. Hasegawa, T. Sato, K. Kanamori, K. Nakano, T. Yajima, Y. Kobayashi, H. Kageyama, T. Abe and K. Nakanishi, *Chem. Mater.* 2013, **25**, 3504-3512.
16. Y. Shen, D. Ding, Y. Yang, Z. Li and L. Zhao, *Mater. Res. Bull.* 2013, **48**, 2317-2324.
17. Q. Kuang and S. Yang, *ACS Appl. Mater. Interfaces*, 2013, **5**, 3683-3690.
18. Y. Li, N. Koshizaki, H. Wang and Y. Shimizu, *ACS Nano*, 2011, **5**, 9403-9412.
19. G. Nie, X. Lu, J. Lei, L. Yang, X. Bian, Y. Tong and C. Wang, *Electrochim. Acta*, 2013, **99**, 145-151.
20. G. Shi, K. Zhang, S. Zhou and Q. Zhang, *Mater. Lett.* 2013, **107**, 228-230.
21. J. Liu and G. Zhang, *CrystEngComm*, 2013, **15**, 382-389.
22. Z. Yu, X. Wu, J. Wang, W. Jia, G. Zhu and F. Qu, *Dalton T.* 2013, **42**, 4633-4638.
23. X. Yang, J. Fu, C. Jin, J. Chen, C. Liang, M. Wu and W. Zhou, *J. Am. Chem. Soc.* 2010, **132**, 14279-14287.
24. S. Wang, P. Wang, C. Xiao, B. Yao, R. Zhao and M. Zhang, *CrystEngComm*, 2013, **15**, 9170-9175.
25. J. Yang, L. Jiao, Q. Zhao, Q. Wang, H. Gao, Q. Huan, W. Zheng, Y. Wang and H. Yuan, *J. Mater. Chem.* 2012, **22**, 3699-3701.
26. X. He, C. Hu, Q. Yi, X. Wang, H. Hua and X. Li, *Catal. Lett.* 2012, **142**, 637-645.
27. J. Li, J. Huang, C. Yu, J. Wu, L. Cao and K. Yanagisawa, *Chem. Lett.* 2011, **40**, 579-581.
28. B. Liu, J. Wang, J. Wu, H. Li, H. Wang, Z. Li, M. Zhou and T. Zuo, *Mater. Lett.* 2013, **91**, 334-337.
29. L. Zhou, J. Zou, M. Yu, P. Lu, J. Wei, Y. Qian, Y. Wang and C. Yu, *Cryst. Growth Des.* 2008, **8**, 3993-3998.
30. J. Li, J. Huang, J. Wu, L. Cao, Q. Li and K. Yanagisawa, *CrystEngComm*, 2013, **15**, 7904-7913.
31. Y.-L. Ma, L. Zhang, X. F. Cao, X.-T. Chen and Z.-L. Xue, *CrystEngComm*, 2010, **12**, 1153-1158.
32. D. M. Griffiths and C. H. Rochester, *J. Chem. Soc., Faraday Trans. 1: Physical Chemistry in Condensed Phases*, 1978, **74**, 403-417.
33. V. H. Pan, T. Tao, J. W. Zhou and G. E. Maciel, *J. Phys. Chem. B*, 1999, **103**, 6930-6943.
34. G. T. Wang, C. Mui, C. B. Musgrave and S. F. Bent, *J. Am. Chem. Soc.* 2002, **124**, 8990-9004.
35. L. Xu, Y. L. Hu, C. Pelligra, C. H. Chen, L. Jin, H. Huang, S. Sithambaram, M. Aindow, R. Joesten and S. L. Suib, *Chem. Mater.* 2009, **21**, 2875-2885.
36. J. Zhang, Sun, Yin, Su, Liao and Yan, *Chem. Mater.* 2002, **14**, 4172-4177.
37. G. T. Wang, C. Mui, C. B. Musgrave and S. F. Bent, *J. Phys. Chem. B*, 2001, **105**, 12559-12565.
38. D. K. Ma, J. L. Jiang, J. R. Huang, D. P. Yang, P. Cai, L. J. Zhang and S. M. Huang, *Chem. Commun.* 2010, **46**, 4556-4558.
39. J. S. Lee and S. C. Choi, *J. Eur. Ceram. Soc.* 2005, **25**, 3307-3314.
40. J. Chojnacka, *J. Inorg. Nucl. Chem.* 1971, **33**, 1345-1363.
41. J. F. Duncan and D. L. Kepert, *J. Chem. Soc. (Resumed)*, 1961, 5317-5325.
42. J. F. Duncan and D. L. Kepert, *J. Chem. Soc. (Resumed)*, 1962, 205-214.
43. X. Li, J. Li, Q. Zhou, Z. Peng, G. Liu and T. Qi, *Metall and Materi Trans B*, 2012, **43**, 221-228.
44. S. Kunjara Na Ayudhya, P. Tonto, O. Mekasuwandumrong, V. Pavarajarn and P. Prasertdam, *Cryst. Growth Des.* 2006, **6**, 2446-2450.
45. Y. G. Yu, G. Chen, L. X. Hao, Y. S. Zhou, Y. Wang, J. Pei, J. X. Sun and Z.-H. Han, *Chem. Commun.* 2013, **49**, 10142-10144.
46. T. Watanabe, T. Takizawa and K. Honda, *J. Phys. Chem.* 1977, **81**, 1845-1851.
47. D. Zhang, J. Wu, B. Zhou, Y. Hong, S. Li and W. Wen, *Nanoscale*, 2013, **5**, 6167-6172.
48. W. Mekprasart, N. Vittayakorn and W. Pecharapa, *Mater. Res. Bull.* 2012, **47**, 3114-3119.
49. T. B. Li, G. Chen, C. Zhou, Z. Y. Shen, R. C. Jin and J. X. Sun, *Dalton T.* 2011, **40**, 6751-6758.
50. J. Zhuang, Q. Tian, H. Zhou, Q. Liu, P. Liu and H. Zhong, *J. Mater. Chem.* 2012, **22**, 7036-7042.